

Article

Effects of Symmetry Restriction on the Antenna Gain Optimized Using Genetic Algorithms

Michael Renzler , Dominik Mair , Markus Hesche and Thomas Ussmueller 

Microelectronics and Implantable Systems Group, Department of Mechatronics, Universität Innsbruck, 6020 Innsbruck, Austria

* Correspondence: michael.renzler@uibk.ac.at

Abstract: Automated design techniques for antennas are highly interesting regarding their ability to cut down on development time and their overall importance for communication technology. Sub-dividing a given area into individual pixels renders methods such as genetic algorithms possible, which enables an automated optimization process by evolutionary methods. While there are many examples in the literature that use this approach, most of them use the reflection coefficient as the optimization goal. Although this yields satisfying antennas for a variety of different applications, this approach generally does not achieve high directivities or antenna gains. In this work, we present the evolutionary optimization of antenna gain for pixelated antennas and the effect of symmetry restriction on the optimized topologies.

Keywords: pixelated antennas; genetic algorithms; automated optimization; symmetry restriction



Citation: Renzler, M.; Mair, D.; Hesche, M.; Ussmueller, T. Effects of Symmetry Restriction on the Antenna Gain Optimized Using Genetic Algorithms. *Symmetry* **2023**, *15*, 658. <https://doi.org/10.3390/sym15030658>

Academic Editors: Wenyin Gong and Libao Deng

Received: 31 January 2023

Revised: 23 February 2023

Accepted: 2 March 2023

Published: 6 March 2023



Copyright: © 2023 by the authors. Licensee MDPI, Basel, Switzerland. This article is an open access article distributed under the terms and conditions of the Creative Commons Attribution (CC BY) license (<https://creativecommons.org/licenses/by/4.0/>).

1. Introduction

Genetic algorithms (GAs) can be used for a variety of different applications, such as scheduling medical appointments [1], industrial clothing design [2] and structural health monitoring [3], but they are particularly useful for solving electromagnetic problems [4]. This has been extensively shown for pixelated or fragmented electromagnetic antennas in recent decades.

Pixelated or fragmented electromagnetic antennas have become an active research area, since they can not only be used for a variety of different application scenarios, but their appearance makes them suitable for automated design processes, such as particle swarm optimization [5–7] or the aforementioned GAs [8–12].

Typically, the reflection coefficient S_{11} is used as a target function for the GA. While this is sufficient to create omnidirectional radiators that can be used for certain Internet of Things applications [13], directional antennas are much more robust against interference from off-axis sources due to their directional selectivity. Other advantages are improved data transmission and more efficient energy harvesting caused by their high gain. This is especially useful in certain energy harvesting application scenarios, such as passive UHF RFID, where devices are solely powered by the electromagnetic radiation from an external transmitter. Previous studies have reported on the gain enhancement of (pixelated) antennas using GAs [14,15]; however, the antenna gain was not used as a target function for optimization. As in other studies, the reflection coefficient was used and the influence of the optimization procedure on the gain was investigated. Examples of studies that have used the antenna gain as an optimization goal include the work of Jayasinghe and Uduwawala [16] and Chiu and Cheng [17].

In addition to the very few studies on the optimization of the gain for pixelated antennas, the effects of symmetry restrictions have also been mostly neglected so far. The only restrictions concerning the topology of pixelated antennas are usually applied to the overall size. In general, any restriction in symmetry decreases the possible solution space, potentially leading to worse results for automated optimization procedures that can be used to

optimize pixelated antennas. Indeed, this has been studied for pixelated phased arrays that have been optimized using genetic algorithms, where the results showed that asymmetric arrays have a better scan and/or bandwidth performance [18]. For conventional antennas, symmetry restrictions have been demonstrated to influence the matching in asymmetric dipoles due to an increased radiation resistance [19] and the design of Baluns [20].

This study focuses on the optimization of the antenna gain, while also investigating the effects of symmetry restrictions for exemplary antennas in the UHF RFID band, with a resonance frequency of 868 MHz. Using an automated optimization procedure employing genetic algorithms, antennas of different symmetry can be specifically optimized for their antenna gain or power in an automated manner.

This is the first report on the effects of symmetry restriction on the gain of pixelated antennas that have been optimized using genetic algorithms. The results show that it is advantageous to not apply any symmetry restriction for electrically large antennas. Specifically, unrestricted optimization enables the generation of high gain antennas without sacrificing the reflection coefficient.

2. Methods

The presented optimization method and measurement procedure have been described in detail in previous studies [13,21], which is why only a short summary will be given here.

The optimization method is implemented in Matlab and uses the *ga*-function as the genetic algorithm. The pixelation process, generation of the (initial) population and optimization are handled within Matlab. The simulation of the desired parameters, such as radiated power or gain for the generated antenna structures, is achieved using Sonnet Software via the Sonnetlab Toolbox [22].

2.1. Pixelation

In order to achieve an automated optimization procedure using a genetic algorithm, a predefined area has to be subdivided into individual elements or pixels, as indicated in Figure 1. Each pixel is represented by a Boolean value that corresponds to a conductive or non-conductive element (0, 1). A conductive element, or “1”, is analogous to a 35 μm thick copper layer on top of the substrate (Rogers RO4350B). Although any geometrical shape can be used, crosses have been shown to be advantageous over rectangles and hexagons for mainly two reasons:

1. Singularities: for rectangles, infinitesimally small connections between pixels can occur (Figure 1a). This can lead to a diminished simulation accuracy and also errors in measurements due to a limited production accuracy.
2. Resolution: restriction to rectangular cells for the simulation mesh in certain software packages leads to errors due to the limited resolution of the angled sides in hexagons (Figure 1c).

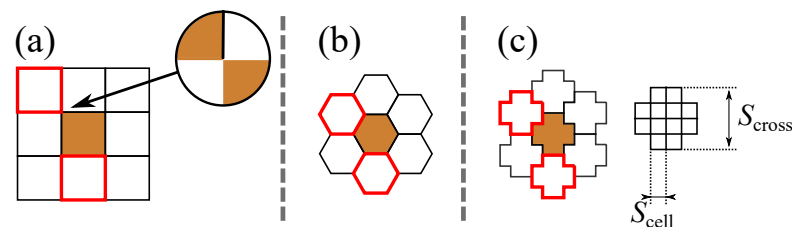


Figure 1. Possible connections between elements of different shapes: (a) rectangles, (b) hexagons and (c) crosses, where red elements show vertical and diagonal neighbors. Diagonal elements can result in singularities due to a (theoretically) infinitesimally small connection (a), whereas for vertically spaced elements no singularities occur (b,c). For cross-shaped elements, the cross size (S_{Cross}) is defined as well as its separation into different Sonnet Software cells with size S_{cell} (c).

Crosses exhibit no singularities and are ideal for simulation tools that employ rectangular cells. Every second row is shifted by half an element in order to avoid non-conducting areas between the crosses. The minimum resolution has been found to be 0.58% of the wavelength, i.e., a more refined mesh does not lead to improved simulation results.

2.2. Genetic Algorithm

The basic principle of genetic algorithms, as shown in Figure 2, is the optimization of a problem through the continued improvement or evolution of individuals.

1. Based on user input, a given antenna size is pixelated and a first, random, initial population with a uniform distribution of pixels (50% "0" and 50% "1") is generated in Matlab.
2. This initial population is simulated with Sonnet Software, which has been chosen due to its fast computation time. Parameters needed for the calculation of a fitness function (i.e., reflection coefficient and gain or power) are simulated for each individual of the population and handed back to Matlab.
3. The fitness function for each individual is computed from these simulated parameters, after which evolutionary methods such as selection, recombination and mutation are used to create a second population.
4. The second population is again simulated with Sonnet Software.

This iterative process is repeated until either the termination criterion has been achieved (e.g., the desired optimization goal) or the maximum number of generations has been reached.

Post-optimization simulations are carried out employing full wave simulations with Ansys HFSS to cross-check the achieved results with Sonnet Software.

2.2.1. Antenna Parameters

In contrast to previous studies by the authors, instead of a low reflection coefficient S_{11} , the antenna gain or power are chosen as an optimization goal.

Both directivity, D , and gain, G , are a measure of the increase in emitted power over a reference antenna (isotropic antenna with uniform radiation in all spatial directions) in a specific direction.

The directivity function is defined as the ratio between the power per unit solid angle at a specific angle $U(\Theta, \varphi)$ and the average radiated power per unit solid angle $P_{rad}/(4\pi)$ [23].

$$D(\Theta, \varphi) = \frac{U(\Theta, \varphi)}{\frac{1}{4\pi} P_{rad}} \quad (1)$$

The gain function additionally takes the radiation efficiency, η_r , into consideration [23].

$$G(\Theta, \varphi) = \frac{U(\Theta, \varphi)}{\frac{1}{4\pi} P_{rad}} \eta_r = D(\Theta, \varphi) \eta_r \quad (2)$$

If not specified otherwise, the maximum value of Equation (1) is called the *directivity* and the maximum of Equation (2) is called the *gain*. Both are given in dBi when compared to an isotropic radiator.

The radiation efficiency can be defined as

$$\eta_r = \frac{P_{rad}}{P_a} \quad (3)$$

with P_a being the power accepted by an antenna, which can be written as:

$$P_a = P_t - P_r \quad (4)$$

where P_r is the reflected power due to impedance mismatch and P_t is the transmitted power to the antenna.

Using powers, the reflection coefficient S_{11} can be defined as follows:

$$|S_{11}|^2 = \frac{P_r}{P_t} \quad (5)$$

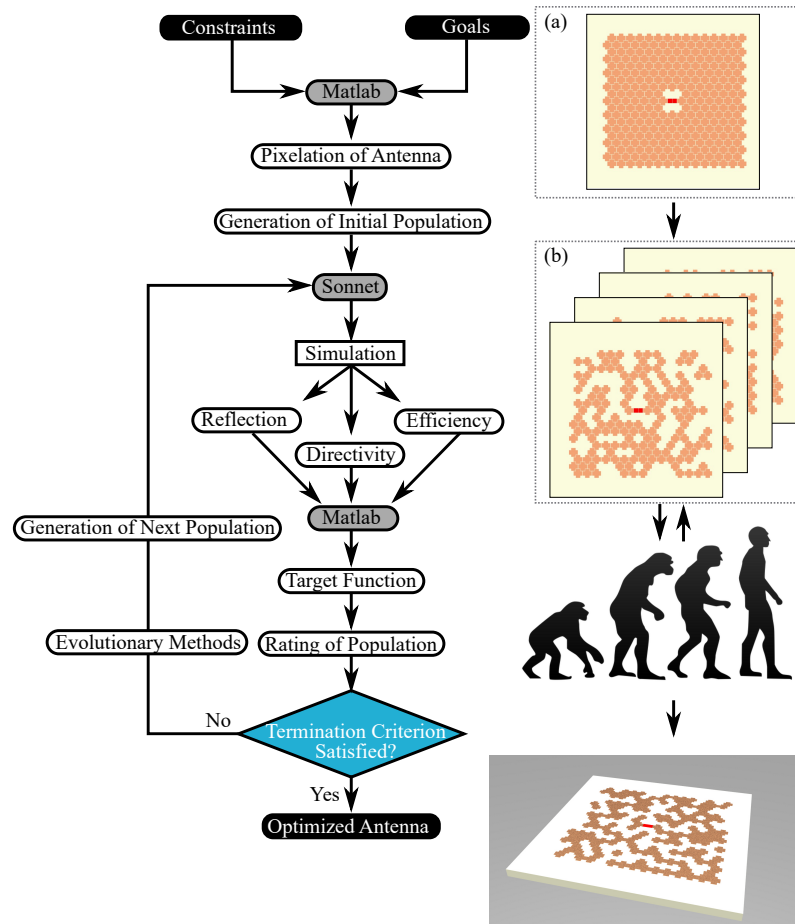


Figure 2. Flowchart of the proposed optimization technique. Initially, a predefined area is pixelated (a), after which an initial population is created with Matlab (b). After simulation with Sonnet, the fitness function is computed in Matlab. The population is rated and if it does not meet the termination criteria, a new one is created based on the first optimization.

2.2.2. Symmetry Restriction

In order to study the influence of symmetry restrictions on an antenna's performance, four distinct cases have to be distinguished:

- (a) Asymmetry: no symmetry restrictions are applied to the antenna;
- (b) x-symmetry: the antenna is symmetrical along the x-axis;
- (c) y-symmetry: the antenna is symmetrical along the y-axis;
- (d) xy-symmetry: the antenna is symmetrical along both axes.

Figure 3 shows exemplary representations of pixelated structures with different symmetries. The point of origin at (0, 0) in green indicates the antenna port, where differential feeding to the antenna is applied.

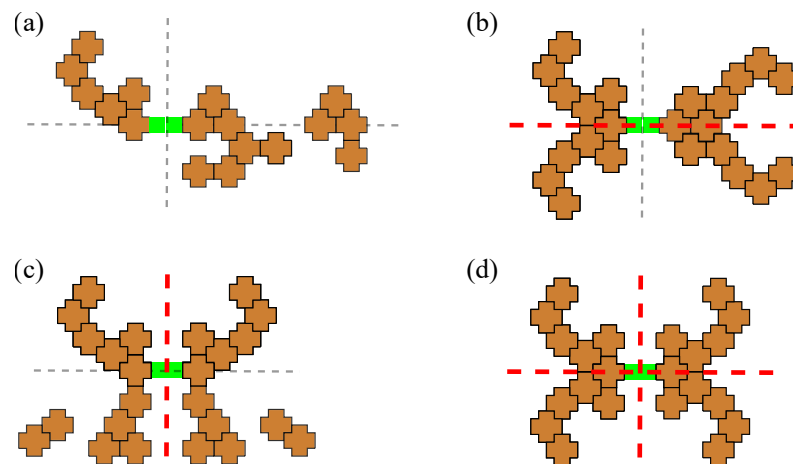


Figure 3. Examples of the different antennas: asymmetrical (a), symmetrical along the x-axis (b), symmetrical along the y-axis (c) and symmetrical along both x- and y-axes (d). The dashed red lines indicate the symmetry axes. The green elements in the center of the antenna indicate the antenna port.

2.3. Measurement Procedure

Prior to the measurement, a VNA (Rohde und Schwarz, ZNB-8) is calibrated using through-open-short-match (TOSM) calibration (Rohde und Schwarz, ZV-Z170). For gain measurements, each antenna is measured twice (in the horizontal and vertical directions) to obtain the total system gain. In order to avoid pattern squint due to unbalanced currents, a Bazooka Balun is used, whose length is shorter than a quarter wavelength because of fringing fields at the open end of the balun [24].

Due to the balanced nature of the produced antennas, the method described by Qing et al. [25] is used to measure the impedance. The “direct compensation” standard de-embedding technique of the employed VNA is used, employing shorted fixture connectors to offset the influence of the test fixture.

3. Results

The main goal of this work was to design directional antennas. Antennas of different types were optimized following the process described above. Relevant data were collected for comparison in the following section. The antennas were optimized using gain or power in either the x-, y- or z-directions. The chosen operating frequency was 868 MHz for operation in the UHF RFID band.

The topologies implemented for this work were x-symmetrical, y-symmetrical and xy-symmetrical electrically large antennas, due to the ease of manufacture and short simulation times.

In order to describe the size of an antenna, the electrical size ka is used, where k is the wavenumber ($2\pi/\lambda$) in radians per meter and a is the radius of a sphere at the antenna’s largest dimension.

$ka \leq 1$ is often used as the threshold for electrically small antennas [26]; therefore, $ka > 1$ describes electrically large antennas in this study.

3.1. Simulation Results

Table 1 shows the physical dimensions and the electrical size of the various types of simulated antennas.

Apart from small deviations due to pixels deleted by the optimization process, the dimensions were kept the same within each group. The optimization options were kept identical across all simulations and are shown in Appendix A, Table A1. The exception is the method of calculating the fitness score, maximum power or maximum gain. The best antenna possible within the allotted generation limit is generated by giving the fitness function a goal it cannot reach.

Table 1. Dimensions and electrical sizes of the groups of generated antennas.

Antenna	Dimensions/mm	Dimension/Pixels	Electrical Size
Asymmetrical	152.5 × 143.75	30 × 38	1.91
x symmetrical	152.5 × 140	30 × 37	1.88
y symmetrical	150 × 143.75	29 × 38	1.89
xy symmetrical	150 × 140	29 × 37	1.87

The antennas were then investigated for the achieved maximum gain, their reflection coefficient at the operating frequency and the radiating direction of the main lobe with the deviation from the desired direction. The resolution of the gain patterns was examined in 5° steps in the θ and ϕ directions, as this delivers precise results in addition to a reasonable computing time. Table A2 in Appendix B shows these parameters at the desired resonance frequency of 868 MHz, in addition to the used target function.

Table 2 summarizes these results by showing the minimal and maximum achieved gain for each antenna symmetry compared to the theoretical gain according to the Chu–Harrington limit [27].

Table 2. Comparison of the calculated Chu–Harrington limit for each antenna type (G_{CH}), the maximum achieved gain (G_{max}) and the minimum achieved gain (G_{min}).

Antenna	G_{CH} /dB	G_{max} /dB	G_{min} /dB
Asymmetrical	7.45	7.76	3.78
x symmetrical	7.31	7.24	4.35
y symmetrical	7.35	7.06	3.57
xy symmetrical	7.22	5.05	6.18

The results for gain and S_{11} are shown in Figure 4, with the respective Chu–Harrington limit for the different antenna topologies. The employed nomenclature is *Date-Symmetry-Direction of Optimization*. The letter “r” for antenna symmetry designates radial symmetry, i.e., the xy symmetry. The colors of the data points in the plot indicate the symmetry of the optimized antennas, whereas the shapes of said data points signify the direction of optimization. Except for 210127aSzO, the gain of all asymmetrical antennas exceeds 5.5 dBi. Conversely, all symmetrical antennas, with the exception of 210116rSyO and 210109ySyO, fall below this threshold.

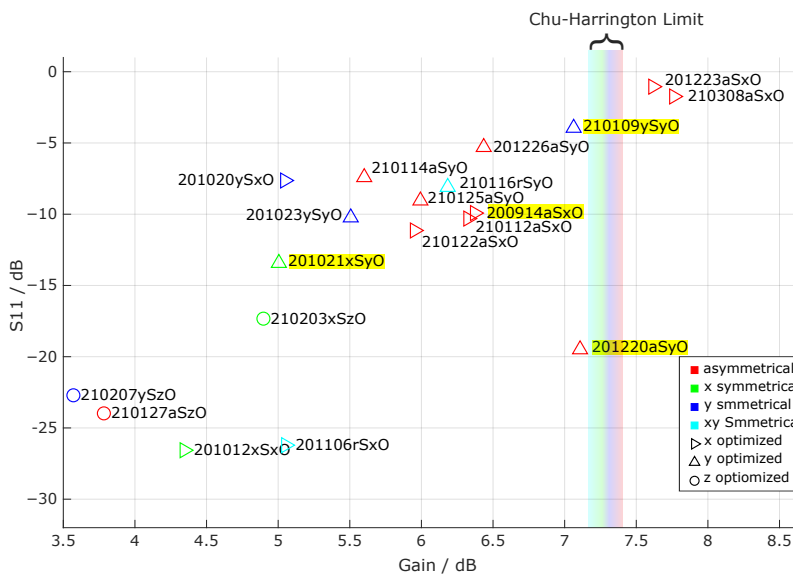


Figure 4. Gain and S_{11} for all optimized antenna structures with their respective symmetry and direction of optimization. The antennas chosen for measurement are highlighted.

Additionally, it can be seen from Table 2 in conjunction with Figure 4 that the only antennas surpassing the Chu–Harrington limit are 201223aSxO and 210308aSxO, which are asymmetric antennas optimized in the x-direction. The gains of all other antennas fall below their respective Chu–Harrington limit.

By looking at Table A2, it is apparent that all antennas with $S_{11} < -5$ dB have been optimized using the power, $U(\Theta, \varphi)$, and not the gain, $G(\Theta, \varphi)$. This is due to the fact that the antenna gain is independent of S_{11} , but not the power $U(\Theta, \varphi)$. Therefore, optimizing for $U(\Theta, \varphi)$ inherently leads to better results for the reflection coefficient, whereas this parameter is not regarded when using $G(\Theta, \varphi)$ as an optimization goal.

Consequently, in order to achieve a high gain and a low reflection coefficient, two possible strategies are possible:

- Optimizing for power;
- Multi-objective optimization to optimize an antenna using gain and S_{11} as target functions at the same time. This method has already been successfully used to optimize pixelated antennas for submersion in dielectric materials in a recent study by the authors [28].

3.2. Measurement Results

Four antennas were chosen for experimental verification based on their high gain and low reflection coefficients: two asymmetrical antennas (201220aSyO and 201111aSxO) and one antenna for each symmetry axis (y-symmetrical: 210109ySyO and x-symmetrical: 201021xSyO). The resulting topologies are shown in Figure 5.

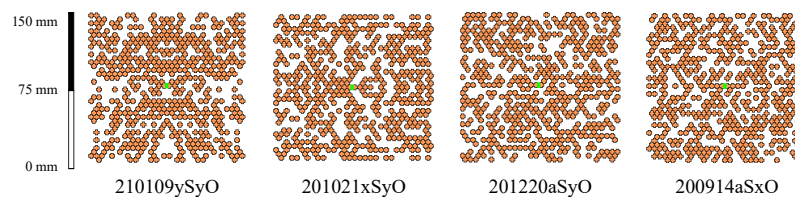


Figure 5. Topologies of the measurements chosen for experimental verification. The green squares indicate the feeding.

The axial ratios of these presented topologies are 87 dB (210109ySyO), 72 dB (201021xSyO), 64 dB (201220aSyO) and 75 dB (201111aSxO), respectively, indicating a strong linear polarization.

The gain patterns, the gain in the desired optimization direction and the S_{11} of each antenna are shown compared to the simulation results. The gain patterns were measured at 868 MHz. Surface current plots of the measured topologies are shown in Appendix C.

3.2.1. Antenna 210109ySyO

Gain Pattern

The measured and simulated data of 210109ySyO are in excellent agreement, as can be seen in Figure 6. Furthermore, the developed directivity matches the direction of optimization. The measured gain in the azimuth plane is 5.99 dBi. The mean absolute error (MAE) of the gain pattern between measurement and simulation is 1.08 dB.

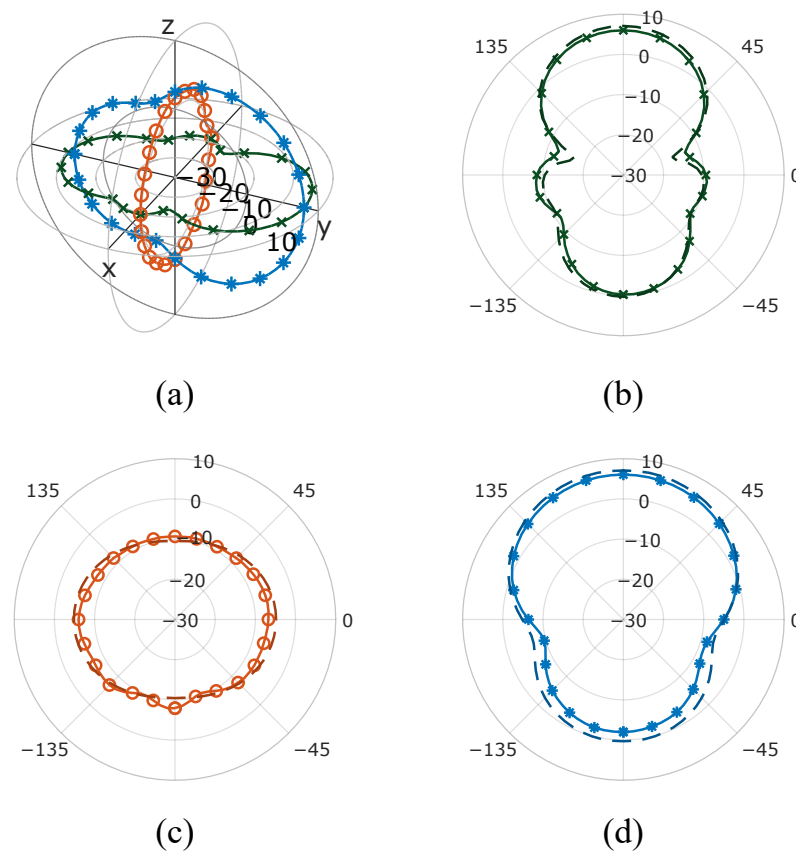


Figure 6. (a) Gain pattern of 210109ySyO in 3D, (b) the azimuth plane and (c) the elevation plane at $\phi = 0^\circ$ and (d) at $\phi = 90^\circ$ (measurement: — simulation: - - -).

S_{11} Parameter

The measured value of S_{11} is -16.98 dB at a resonance frequency of 853.74 MHz, compared to the simulation value of -15.62 dB at 859.94 MHz, as seen in Figure 7. This corresponds to a deviation of only 0.7% between measurement and simulation.

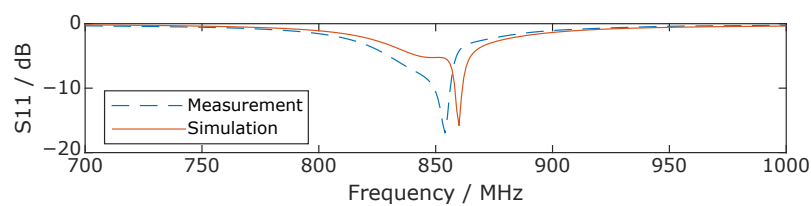


Figure 7. S_{11} of 210109ySyO between 700 MHz and 1 GHz.

3.2.2. Antenna 201021xSyO

Gain Pattern

Again, the measurements match the simulation very well and the developed directivity matches the direction of optimization, as can be seen in Figure 8. The measured gain in the azimuth plane is 3.27 dBi. The MAE of the gain pattern between measurement and simulation is 2.11 dB.

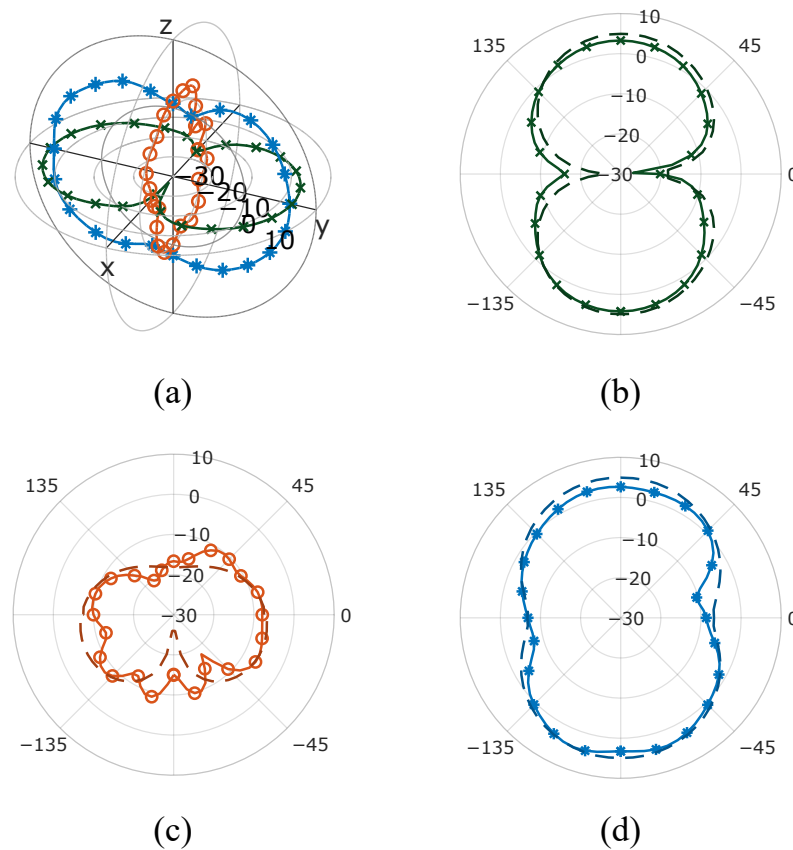


Figure 8. (a) Gain pattern of 210109xSyO in 3d, (b) the azimuth plane and (c) the elevation plane at $\phi = 0^\circ$ and (d) at $\phi = 90^\circ$ (measurement: — simulation: - - -).

S_{11} Parameter

The measured and simulated S_{11} of this antenna are close to being identical, as can be seen in Figure 9. The measured value of S_{11} is -14.52 dB at a frequency of 867.7 MHz, compared to the simulated value of 867.11 MHz.

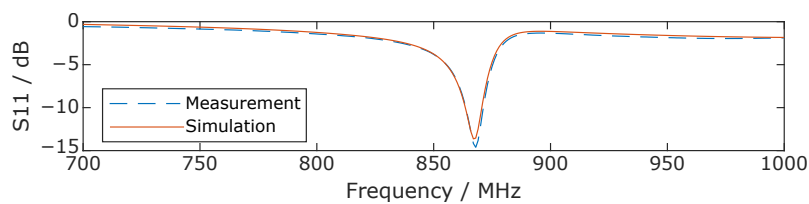


Figure 9. S_{11} of 201021xSyO between 700 MHz and 1 GHz.

3.2.3. Antenna 201220aSyO

Gain Pattern

This antenna is asymmetrical and clearly develops a strong directivity seen in Figure 10, with an overall excellent agreement between measurements and simulations. The measured gain in the elevation plane ($\phi = 90^\circ$) is 6.31 dBi and the MAE of the gain pattern between measurement and simulation is 1.65 dB.

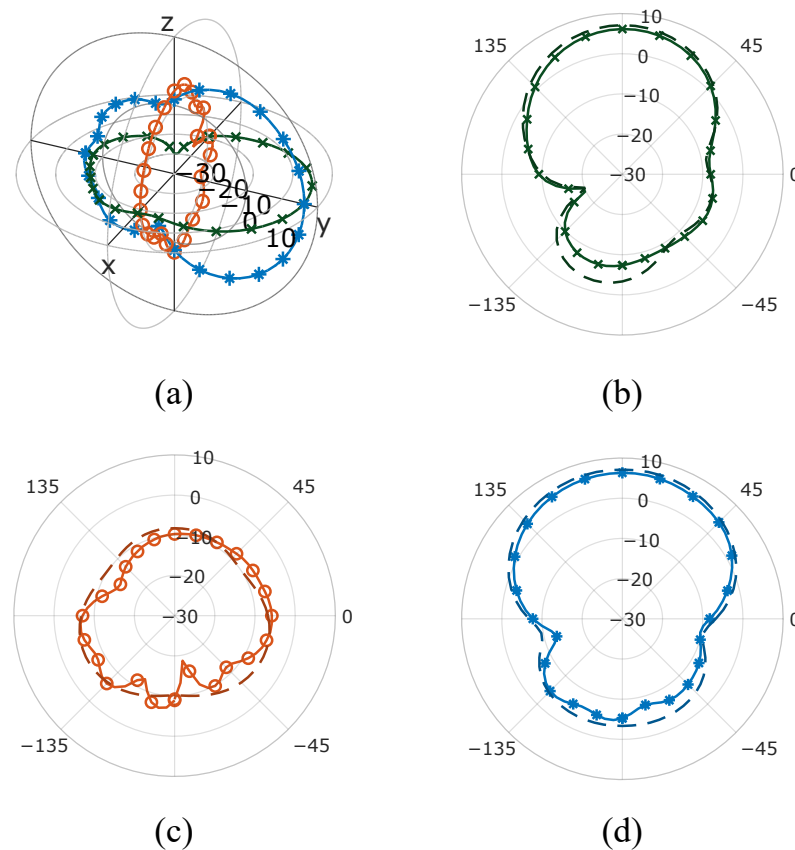


Figure 10. (a) Gain pattern of 201220aSyO in 3d, (b) the azimuth plane and (c) the elevation plane at $\phi = 0^\circ$ and (d) at $\phi = 90^\circ$ (measurement: — simulation: - - -).

S_{11} Parameter

For this antenna, S_{11} shows the largest deviation (in resonance and value), as seen in Figure 11. The measured value of S_{11} is -13.5 dB at a resonance frequency of 855.74 MHz, compared to the simulation value of -19.58 dB at 869.79 MHz, which corresponds to a deviation of 1.6% between measurement and simulation.

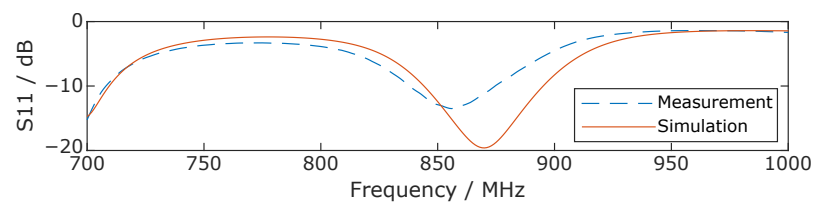


Figure 11. S_{11} of 201220aSyO between 700 MHz and 1 GHz.

3.2.4. Antenna 200914aSxO

Gain Pattern

This antenna was optimized in the x-direction, which can be seen in Figure 12. Slight deviations can be detected in sections with a small gain. The measured gain in the elevation plane ($\phi = 0^\circ$) is 5.21 dBi and the MAE of the gain pattern between measurement and simulation is 2.29 dB.

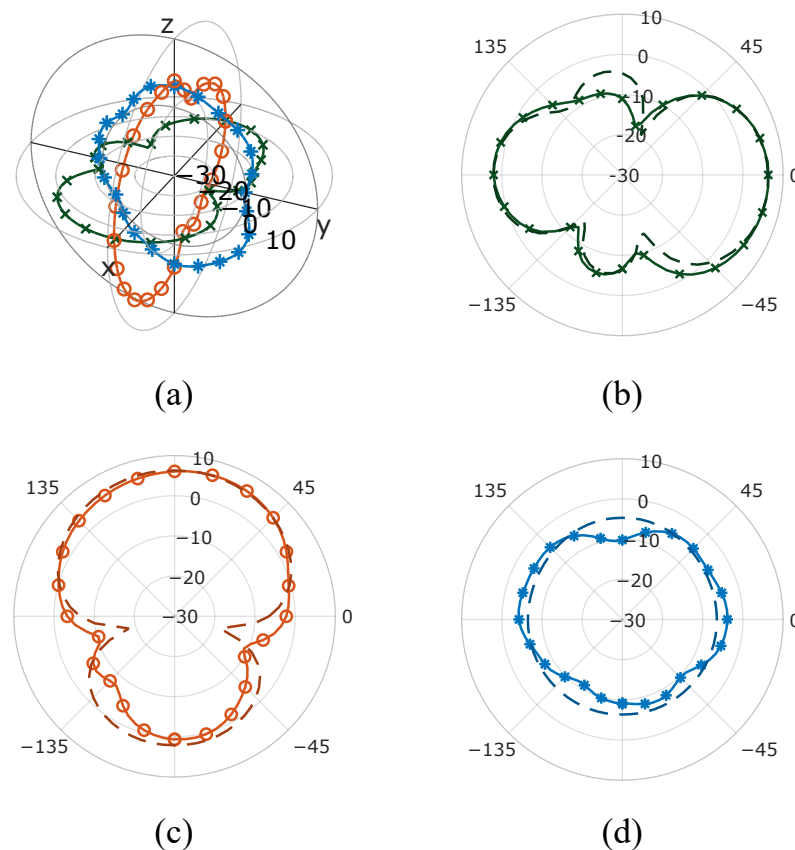


Figure 12. (a) Gain pattern of 200914aSxO in 3d, (b) the azimuth plane and (c) the elevation plane at $\phi = 0^\circ$ and (d) at $\phi = 90^\circ$ (measurement: — simulation: - - -).

S_{11} Parameter

This antenna developed two resonances in the pictured band. At the first resonance, the simulation and measurement match well, and at the second, a downshift in the minimum is visible, Figure 13. The measured value of S_{11} is -11.85 dB at a resonance frequency of 863.73 MHz, compared to the simulated value of -9.92 dB at 864.03 MHz, which is a negligible deviation. The deviation for the second resonance (around 950 MHz) is not discussed, since this was not an optimization goal.

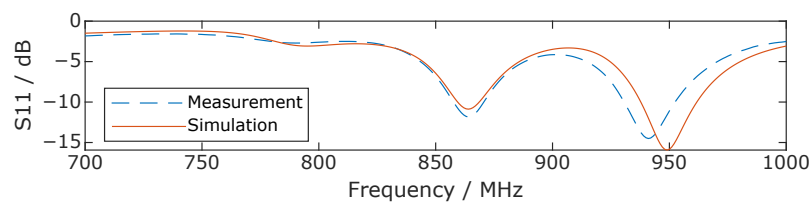


Figure 13. S_{11} of 200914aSxO between 700 MHz and 1 GHz.

3.3. Gain and Radiation Efficiency as a Function of Frequency

Figures 14 and 15 show the radiation efficiency and gain in the frequency range of 700 MHz to 1000 MHz.

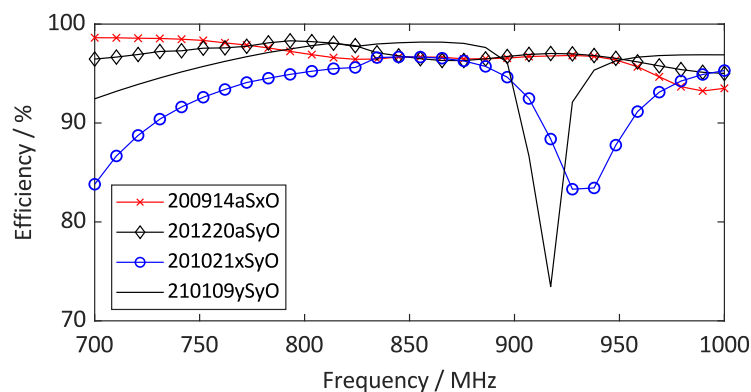


Figure 14. Radiation efficiency as a function of frequency.

While the asymmetric antennas exhibit a consistent efficiency in the investigated frequency range, the symmetric antennas experience considerable dips around 917 MHz (210109ySyO) and 930 MHz (201021xSyO).

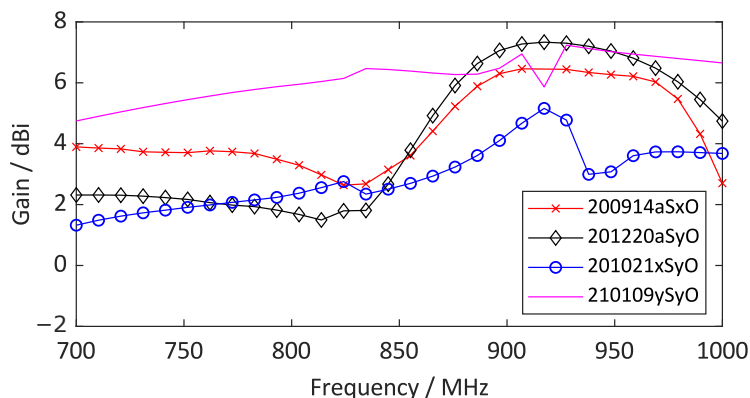


Figure 15. Gain as a function of frequency.

The asymmetric antennas exhibit a clear increase in gain starting from 835 MHz. While the gain of the x-symmetric antenna also slightly increases at this frequency before decreasing again to 920 MHz, the y-symmetric antenna shows a steady, high gain over the whole range.

A more detailed study on this behavior must be performed, possibly also employing multi-objective optimization in order to test these properties for a larger dataset. For just the four measured antennas, no clear statements about the influence of symmetry restrictions on the gain and radiation efficiency can be made. A common mode analysis of symmetric antennas might also yield additional information on the behaviour of the radiation efficiency for symmetric antennas.

Differences in the results for gain versus frequency and gain patterns shown in the previous paragraphs are due to the fact that the frequency dependence was simulated using Ansys, whereas the gain patterns were simulated using Sonnet due to the lower computation time.

4. Discussion

Overall, the simulated data match the measurement results very well, as extensively documented in Section 3.2. The errors between measured and simulated resonance frequencies are very small, with the highest deviation being 1.6%. The measured gain patterns match the simulated data very well, with the development of directional antennas in the desired direction of optimization. The simulation results were confirmed and the overall premise of the presented study, i.e., symmetry restrictions and their effects on the antenna gain, was shown to lead to interesting insights for pixelated antennas.

Optimizing for power or gain produces highly directional antennas, with gains close to the theoretical Chu–Harrington limit. This is the first report on pixelated antennas that have been specifically optimized for high gain by using either the gain or power as a target function in a genetic algorithm. A clear deviation in results is seen between choosing gain or power as the target function, where the latter can also produce well-matched antennas, i.e., those with a low S_{11} and a high gain at the same time. Using the gain as an optimization goal leads to unsatisfying results for the reflection coefficient. As discussed in Section 3.1, this is due to the fact that the antenna gain is independent of S_{11} , whereas $U(\Theta, \varphi)$ is not.

In order to achieve high-gain, well-matched antennas, optimizing for power is the method of choice when using single objective optimization. Multi-objective optimization of gain and reflection coefficients will be investigated in future studies.

Another possibility that has been shown in a different context for the design of a low-noise stable broadband microwave amplifier [29] is to use a hybrid optimization scheme. In the above study, a genetic algorithm was used in combination with a conjugate gradient method (CGM). While a CGM is not expected to be useful for the optimization of pixelated antennas due to the high dimensionality of the problem, a combination of different optimization methods might yield interesting results for pixelated antennas.

In addition to gain and power, symmetry restrictions were also investigated for antennas that are symmetrical along the x -, y - and xy -axes, and for antennas that have no symmetry restrictions. The results show that unrestricted optimization can lead to antennas that can outperform the Chu–Harrington limit. Therefore, symmetry restriction shows no benefit for electrically large antennas. The applicability of the reported results and their use for electrically small antennas will be studied in future investigations. In previous studies by the authors, it has been shown that electrically small antennas can be optimized for their reflection coefficient [21]. It can be expected that electrically small antennas will benefit from multi-objective optimization, leading to high gain while achieving a low S_{11} .

Another aspect that must be studied in the context of symmetry restrictions is the bandwidth. Preliminary results indicate that the simulated electrically large antennas have narrow bandwidths, but no detailed investigation has been undertaken thus far. While the presented results can be used for the design of other antennas for radio communication, such as for the 2.4 GHz WiFi band, it must be investigated whether they also hold true for mm wave band (30 GHz to 300 GHz) devices or if different symmetry effects will play a role in this wavelength regime.

This is the first report on the effects of symmetry restrictions on pixelated antennas that have been optimized using genetic algorithms. In conclusion, the optimization of pixelated antennas for gain, using the optimization goals of gain or power, produces highly directional antennas, with symmetry restrictions leading to no positive effect. An increased solution space for asymmetric antennas leads to high gain antennas with pronounced directivity, with measurement results confirming the extensive simulations.

Author Contributions: Conceptualization, M.R. and D.M.; methodology, M.R., D.M. and M.H.; software, D.M. and M.H.; validation, M.R., D.M. and M.H.; formal analysis, M.R. and D.M.; investigation, D.M. and M.H.; resources, M.R. and D.M.; data curation, M.R., D.M. and M.H.; writing—original draft preparation, M.R.; writing—review and editing, M.R. and D.M.; visualization, M.R. and M.H.; supervision, M.R., D.M. and T.U.; project administration, M.R.; funding acquisition, M.R. and D.M. All authors have read and agreed to the published version of the manuscript.

Funding: This research was partially funded by the University of Innsbruck.

Institutional Review Board Statement: Not applicable.

Informed Consent Statement: Not applicable.

Data Availability Statement: Not applicable.

Conflicts of Interest: The authors declare no conflict of interest. The funders had no role in the design of the study; in the collection, analyses, or interpretation of data; in the writing of the manuscript; or in the decision to publish the results.

Abbreviations

The following abbreviations are used in this manuscript:

PSO	Particle swarm optimization
GA	Genetic algorithm
MAE	Mean absolute error
GCM	Conjugate gradient method

Appendix A. Optimization Settings

Table A1. Parameters used for the genetic algorithm function within Matlab.

Property	Value
Strings per Generation	50
Crossover Rate	0.8
Mutation Rate	0.01
Elite Count	2
MaxGenerations	200

Appendix B. Simulation Results

Table A2. The gain, reflection coefficient, the direction with the deviation from the desired direction and the optimization goal of all antennas. For antennas optimized in z-direction, no deviation $d\Phi$ can be defined (\sim).

Names	S_{11}/dB	Gain/dB	Θ	$d\Theta$	Φ	$d\Phi$	Target Function
200914aSxO	-9.921	6.373	85	5	355	5	power
201012xSxO	-26.565	4.346	45	45	0	0	power
201020ySxO	-7.635	5.047	85	5	0	0	power
201021xSyO	-13.429	5.005	90	0	90	0	power
201023ySyO	-10.235	5.507	85	5	90	0	power
201106rSxO	-26.209	5.054	5	85	0	0	power
201220aSyO	-19.493	7.108	90	0	90	0	power
201223aSxO	-1.05	7.618	90	0	5	5	gain
201226aSyO	-5.295	6.435	90	0	90	0	gain
210109ySyO	-3.945	7.063	90	0	90	0	gain
210112aSxO	-10.305	6.326	90	0	5	0	power
210114aSyO	-7.409	5.601	85	5	95	5	power
210116rSyO	-8.094	6.184	90	0	90	0	power
210122aSxO	-11.141	5.953	90	0	15	15	power
210125aSyO	-9.048	5.993	90	0	90	0	power
210127aSzO	-23.978	3.783	10	10	225	\sim	power
210203xSzO	-17.33	4.897	5	5	0	\sim	power
210207ySzO	-22.709	3.57	10	10	270	\sim	power
210308aSxO	-1.738	7.763	90	0	5	5	gain

Appendix C. Surface Current Plots

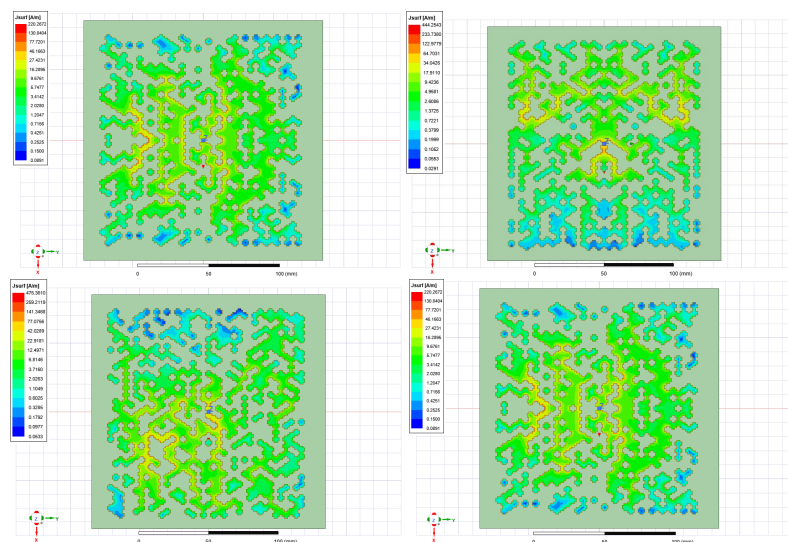


Figure A1. Surface current plots of the measured antennas.

References

1. Squires, M.; Tao, X.; Elangovan, S.; Gururajan, R.; Zhou, X.; Acharya, U.R. A novel genetic algorithm based system for the scheduling of medical treatments. *Expert Syst. Appl.* **2022**, *195*, 116464. [\[CrossRef\]](#)
2. Zhang, X.; Yang, C. Application of Multipopulation Genetic Algorithm in Industrial Special Clothing Design. *Wirel. Commun. Mob. Comput.* **2022**, *2022*, 1632063. [\[CrossRef\]](#)
3. Marasco, G.; Piana, G.; Chiaia, B.; Ventura, G. Genetic Algorithm Supported by Influence Lines and a Neural Network for Bridge Health Monitoring. *J. Struct. Eng.* **2022**, *148*, 04022123. [\[CrossRef\]](#)
4. Weile, D.; Michielssen, E. Genetic algorithm optimization applied to electromagnetics: A review. *IEEE Trans. Antennas Propag.* **1997**, *45*, 343–353. [\[CrossRef\]](#)
5. Dong, J.; Li, Q.; Deng, L. Design of Fragment-Type Antenna Structure Using an Improved BPSO. *IEEE Trans. Antennas Propag.* **2018**, *66*, 564–571. [\[CrossRef\]](#)
6. Jia, X.; Lu, G. A Hybrid Taguchi Binary Particle Swarm Optimization for Antenna Designs. *IEEE Antennas Wirel. Propag. Lett.* **2019**, *18*, 1581–1585. [\[CrossRef\]](#)
7. Aldhafeeri, A.; Rahmat-Samii, Y. Brain storm optimization for electromagnetic applications: Continuous and discrete. *IEEE Trans. Antennas Propag.* **2019**, *67*, 2710–2722. [\[CrossRef\]](#)
8. Haupt, R.L. Thinned arrays using genetic algorithms. *IEEE Trans. Antennas Propag.* **1994**, *42*, 993–999. [\[CrossRef\]](#)
9. Ares-Pena, F.J.; Rodriguez-Gonzalez, J.A.; Villanueva-Lopez, E.; Rengarajan, S.R. Genetic algorithms in the design and optimization of antenna array patterns. *IEEE Trans. Antennas Propag.* **1999**, *47*, 506–510. [\[CrossRef\]](#)
10. Thors, B.; Steyskal, H.; Holter, H. Broad-band fragmented aperture phased array element design using genetic algorithms. *IEEE Trans. Antennas Propag.* **2005**, *53*, 3280–3287. [\[CrossRef\]](#)
11. Ouedraogo, R.O.; Tang, J.; Fuchi, K.; Rothwell, E.J.; Diaz, A.R.; Chahal, P. A tunable dual-band miniaturized monopole antenna for compact wireless devices. *IEEE Antennas Wirel. Propag. Lett.* **2014**, *13*, 1247–1250. [\[CrossRef\]](#)
12. Trinh-Van, S.; Yang, Y.; Lee, K.Y.; Hwang, K. A Wideband Circularly Polarized Pixelated Dielectric Resonator Antenna. *Sensors* **2016**, *16*, 1349. [\[CrossRef\]](#)
13. Mair, D.; Unterladstaetter, M.; Renzler, M.; Ussmueller, T. Evolutionary Optimized Pixelated Antennas for 5G IoT Communication. In Proceedings of the 2022 52nd European Microwave Conference (EuMC), Milan, Italy, 27–29 September 2022; IEEE: New York, NY, USA, 2022. [\[CrossRef\]](#)
14. Derbal, M.C.; Zeghdoud, A.; Nedil, M. A Novel Dual Band Antenna Design for WiFi Applications Using Genetic Algorithms. In Proceedings of the 2018 IEEE International Symposium on Antennas and Propagation & USNC/URSI National Radio Science Meeting, Boston, MA, USA, 8–13 July 2018; IEEE: New York, NY, USA, 2018. [\[CrossRef\]](#)
15. Dhakshinamoorthi, M K.; Gokulakrishna, S.; Denesh Kumar, M.; Subha, M.; Mekaladevi, V. Rectangular Microstrip Patch Antenna Miniaturization using improvised Genetic Algorithm. In Proceedings of the 2020 4th International Conference on Trends in Electronics and Informatics (ICOEI)(48184), Tirunelveli, India, 15–17 June 2020; IEEE: New York, NY, USA, 2020. [\[CrossRef\]](#)
16. Jayasinghe, J.; Uduwawala, D. Optimization of the performance of patch antennas using genetic algorithms. *J. Natl. Sci. Found. Sri Lanka* **2013**, *41*, 113. [\[CrossRef\]](#)

17. Chiu, Y.H.; Chen, Y.S. Multi-objective optimization for UWB antennas in impedance matching, gain, and fidelity factor. In Proceedings of the 2015 IEEE International Symposium on Antennas and Propagation & USNC/URSI National Radio Science Meeting, Vancouver, BC, Canada, 19–24 July 2015; IEEE: New York, NY, USA, 2015. [CrossRef]
18. Steyskal, H. On the Merit of Asymmetric Phased Array Elements. *IEEE Trans. Antennas Propag.* **2013**, *61*, 3519–3524. [CrossRef]
19. Song, C.; Huang, Y.; Zhou, J.; Carter, P.; Yuan, S.; Xu, Q.; Fei, Z. Matching Network Elimination in Broadband Rectennas for High-Efficiency Wireless Power Transfer and Energy Harvesting. *IEEE Trans. Ind. Electron.* **2017**, *64*, 3950–3961. [CrossRef]
20. McLean, J.S.; Foltz, H.D. Symmetry Versus Balance in Balancing Networks for Dipolar Antennas. *IEEE Trans. Electromagn. Compat.* **2020**, *62*, 1406–1418. [CrossRef]
21. Mair, D.; Renzler, M.; Pfeifhofer, A.; Ußmüller, T. Evolutionary optimization of asymmetrical pixelated antennas employing shifted cross shaped elements for UHF RFID. *Electronics* **2020**, *9*, 1856. [CrossRef]
22. Sonnet. SonnetLab. 2023. Available online: <https://www.sonnetsoftware.com/support/sonnet-suites/sonnetlab.html> (accessed on 25 January 2023).
23. Volakis, J.L. *Antenna Engineering Handbook*, 4th ed.; McGraw-Hill Professional: New York, NY, USA, 2007.
24. Saario, S.A.; Lu, J.W.; Thiel, D.V. Full-wave analysis of choking characteristics of sleeve balun on coaxial cables. *Electron. Lett.* **2002**, *38*, 304–305. [CrossRef]
25. Qing, X.; Goh, C.K.; Chen, Z.N. Impedance Characterization of RFID Tag Antennas and Application in Tag Co-Design. *IEEE Trans. Microw. Theory Tech.* **2009**, *57*, 2017288. [CrossRef]
26. Wheeler, H.A. Fundamental limitations of small antennas. *Proc. IRE* **1947**, *35*, 1479–1484. [CrossRef]
27. Harrington, R.F. Effect of antenna size on gain, bandwidth, and efficiency. *J. Res. Nat. Bur. Stand* **1960**, *64*, 1–12. [CrossRef]
28. Mair, D.; Fischer, M.; Konzilia, J.; Renzler, M.; Ussmueller, T. Evolutionary Optimization of Antennas for Structural Health Monitoring. *IEEE Access* **2023**, *11*, 4905–4913. [CrossRef]
29. Shirkolaei, M.M. A New Design Approach of Low-Noise Stable Broadband Microwave Amplifier Using Hybrid Optimization Method. *IETE J. Res.* **2020**, *68*, 4160–4166. [CrossRef]

Disclaimer/Publisher’s Note: The statements, opinions and data contained in all publications are solely those of the individual author(s) and contributor(s) and not of MDPI and/or the editor(s). MDPI and/or the editor(s) disclaim responsibility for any injury to people or property resulting from any ideas, methods, instructions or products referred to in the content.